



Laguerre–Gaussian induced temperature and refractive index profiles in thermal lens effect

ABDUL RAHMAN,¹  HUMBERTO CABRERA,²  MUHAMMAD USMAN MALIK,¹ AND IMRANA ASHRAF^{1,2,*}

¹Department of Physics, Quaid-i-Azam University, Islamabad 44000, Pakistan

²Optics Lab., The Abdus Salam International Center for Theoretical Physics, Strada Costiera 11, 34151, Trieste, Italy

*Corresponding author: drimrana@comsats.net.pk

Received 15 May 2020; revised 25 October 2020; accepted 27 October 2020; posted 27 October 2020 (Doc. ID 397809); published 2 December 2020

In this work, we present a theoretical model that describes induced temperature and refractive index profiles generated by the Laguerre–Gaussian (LG) excitation beam. A comparison between LG and conventional fundamental mode TEM₀₀ is drawn. It indicates that there is a decrease or increase around the optical axis ($z, r = 0$) in the refractive index by LG₁⁰ and LG₀⁵, thus enabling an enhancement of the refractive index gradient along the radius r . The temperature and refractive index profiles produced by the higher-order LG modes are compared with those of a conventional fundamental TEM₀₀ Gaussian beam. The results indicate that there is an increase along the radius in the refractive index gradient generated by LG₁⁰ and LG₀⁵, which could enhance the sensitivity in photothermal lens detection. © 2020 Optical Society of America

<https://doi.org/10.1364/JOSAB.397809>

1. INTRODUCTION

The photothermal effect is a well-known phenomenon commonly used in photothermal spectroscopy. The general principle of operation of all photothermal methods relies on the generation of heat by periodical excitation of the sample. Sensing of the refractive index, pressure, or temperature changes produced after non-radiative de-excitation of absorbed light is the main detection mechanism in photothermal spectroscopy. In the case of thermal lens spectroscopy (TLS), the energy absorbed by the sample is converted into heat, generating a temperature gradient in the sample and consequently a refractive index gradient that causes defocusing of the probe laser beam passing through a liquid pre-excited medium [1–3]. Because of defocusing, the intensity profile of the probe laser beam changes periodically, thus producing a thermal lens (TL) signal, which depends linearly on the absorbance of the sample [4–6]. The TL effect was discovered by Gordon *et al.* [7] while they were measuring the Raman emission spectrum of a liquid inserted inside the laser cavity of a He–Ne laser. In 1973, a theory was developed [8] to describe the TL signal and its dependence on the temperature and refractive index gradients as well as the relationship with the photothermal parameters of the sample. In this work, they observed TL signals in weak-absorbing materials when the liquid sample was placed outside the laser cavity. The main advantages of using the TLS is that the sensitivity is orders of magnitude greater than the conventional UV–Vis spectrometry. Second, TLS is a scattering-free method, enabling more accurate low absorbance measurement. Solomini *et al.*

[9] measured absorption coefficients of more than 27 organic liquids using a single beam TL setup. Later on, Grabiner *et al.* [10] studied the vibrational relaxation phenomena in CH₃F, CH₃Cl, and C₂H₄ using time-resolved TL measurements. However, the previously mentioned works used a single beam configuration in which the laser acts as both excitation and probe beams. Further improvement has been done using a double beam configuration, thus enabling a wavelength scan for spectra measurements [11,12]. This fact allows the use of a fixed probe beam wavelength in the visible part of the spectrum where most detectors are more sensitive and with less interference noise.

Previously, any existing TL theoretical model used the fundamental TEM₀₀ beam as an excitation source. Moreover, there is no theoretical model describing a cw-laser-induced temperature and refractive index profiles produced by higher-order Gaussian modes. During the last few years, physicists have paid considerable attention to particular features and applications of specific intensity profiles of laser beams, i.e., higher-order Laguerre–Gaussian (LG) modes [13,14]. They are used widely as spatial bases and are eigen-functions of the Fourier transform, solutions to the paraxial wave equation, and eigen-modes of quantum harmonic oscillators. For these reasons, LG modes play an important role in many scientific disciplines as well as in theoretical models in physics. LG modes are used in high-precision interferometry for gravitation waves detection [15], spiral phase imaging microscopy [16], to trap ultracold atoms [17], and in microscopy for imaging when spatial filtering is

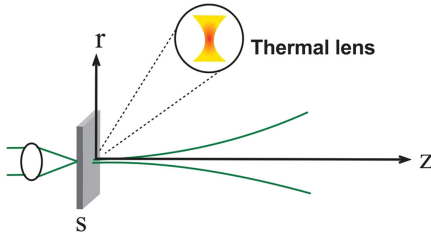


Fig. 1. Schematic of beam propagation.

needed [18]. LG beams present very particular features that seem to be advantageous for TLS. For example, they have intensity profiles with narrower FWHM and higher intensity on the axis that could generate strong refractive index gradients as well as TLS signals. Additionally, the technology associated with the generation and detection of LG modes has a tendency to grow. The Hermite–Gaussian basis can in turn easily be transformed to LG through two cylindrical lenses, and the Gaussian basis can be transformed into LG by means of a spatial light modulator. Thus, the first step that must be considered to obtain a description of the TL signal, generated by LG beams, is to measure the temperature and refractive index changes.

The goal of this paper is to solve analytically the temperature and refractive index gradients generated when the TL effect is produced by high-order Gaussian modes such as LG. The described temperature and refractive index profiles are compared with those generated by the TEM₀₀ Gaussian mode.

2. THEORETICAL MODEL

The model is based on a LG excitation beam propagating in z direction, passing through an absorbing medium of length l , in which the heat flow occurs in radial direction (x , y) and convection effects are negligible. The beam is focused by a converging lens so that it is focused onto the sample with a Rayleigh parameter larger than the length of the sample. The location of the sample is at the waist of the excitation beam and is taken as the origin along the z axis, as shown in Fig. 1. The beam is turned on at time $t = 0$, and the temperature gradient is developed along the radius r . Keeping in mind the cylindrical nature of our problem, we use LG mode beams to excite the sample.

3. TEMPERATURE GRADIENT BY LG_{*l*^{*p*}} MODES

In general, the LG beam LG_{*l*^{*p*}} has a transverse intensity profile. The superscript l describes the angular degree of freedom, while the subscript p is related to the radial profile of the beam (radial nodes). It contains a phase front of spiral shape with a phase shift $2\pi l$ around the circumference of the beam with l negative or positive. For the sake of simplicity, we ignored the negative sign in our calculations. LG_{*l*^{*p*}} can be generated by transforming the fundamental Gaussian mode by using the proper optical element with different techniques. One of these techniques is called the binary phase diffractive optical element (BPDOE) [19]. Its calculations are based on Fresnel–Kirchhoff integrals.

The transverse intensity of a LG beam is represented as follows [20]:

$$I_p^l = \frac{2p!}{(1+p)\pi} \frac{P_0}{w^2} \left(\frac{2r^2}{w^2}\right)^{|l|} \exp\left(\frac{-2r^2}{w^2}\right) \left(L_p^{|l|}\left(\frac{-2r^2}{w^2}\right)\right)^2, \quad (1)$$

where $w(z)$ is the beam radius, P_0 is the power of the laser beam, and (r, z) are cylindrical coordinates.

The heat generated per unit length per unit time between r and $r + dr$ is

$$Q(r) = 2\pi\alpha I_p^l r dr, \quad (2)$$

where α is the absorption coefficient. Dennemeyer *et al.* [21] calculated a non-steady heat transfer equation, as described by

$$c\rho \frac{\partial}{\partial t} [\Delta T(r, t)] - k\nabla^2 [\Delta T(r, t)] - Q(r) = 0, \quad (3)$$

where c is the specific heat, ρ is the density, and ΔT is the temperature rise produced by the source term $Q(r)$. The boundary conditions to solve this nonlinear equation are:

- far from the beam center in radial distance, temperature change vanishes, i.e., at $r \rightarrow \infty$, $\Delta T = 0$;
- initially, there is no temperature change, i.e., at $t = 0$, $\Delta T = 0$.

We can define a Green function for a temperature problem at radius r and time t for the above-mentioned linear heat source at r_1 and $t = 0$:

$$G(r, r_1, t) = \frac{1}{4\pi tk} \exp\left(-\frac{r_1^2 + r^2}{4Dt}\right) \cdot I_0\left(\frac{2rr_1}{2Dt}\right), \quad (4)$$

where I_0 is the special Bessel function of zeroth order, D is thermal diffusivity, and k is the thermal conductivity of the medium in which the beam is propagating.

The general solution for the heat transfer equation for an infinite sample is [22]

$$\Delta T = \int_0^t \int_0^\infty (Q(r_1)G(r, r_1, t)) dt'. \quad (5)$$

For the intensity of Gaussian mode TEM₀₀, substituting $l = 0$ and $p = 0$ into Eq. (1), we get

$$I_0^0 = \frac{2P_0}{\pi w^2} \exp\left(\frac{-2r^2}{w^2}\right). \quad (6)$$

Now we need to identify equations for the intensity of various lower LG modes. Substituting $l = 1$ and $p = 0$ into Eq. (1) gives the intensity profile of LG_{1⁰}:

$$I_0^1 = \frac{4P_0}{\pi} \frac{r^2}{w^4} \exp\left(\frac{-2r^2}{w^2}\right). \quad (6a)$$

Considering $l = 0$ and $p = 1$ in Eq. (1), we can write the intensity of LG_{1⁰} as

$$I_1^0 = \frac{P_0(1 - 2r^2/w^2)}{\pi w^2} \exp\left(\frac{-2r^2}{w^2}\right). \quad (6b)$$

Similarly, the intensities of LG_{0²}, LG_{0³}, LG_{0⁴}, and LG_{0⁵} modes can be derived from Eq. (1) by substituting corresponding values of l and p :

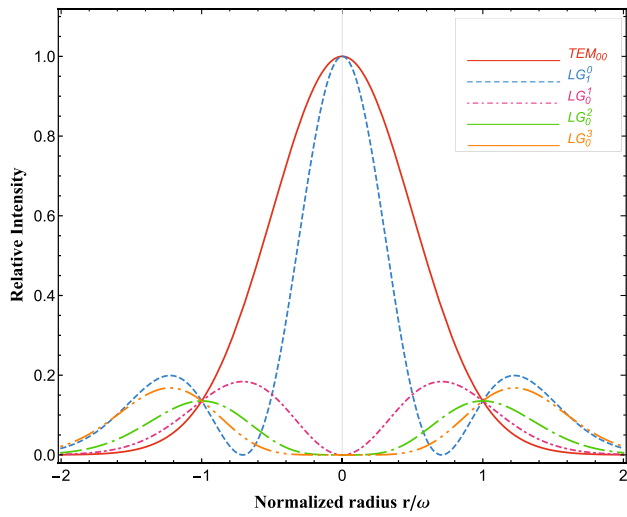


Fig. 2. Radial intensity distribution for various lowest Gaussian and LG modes. The radii are normalized to beam radius of TEM₀₀.

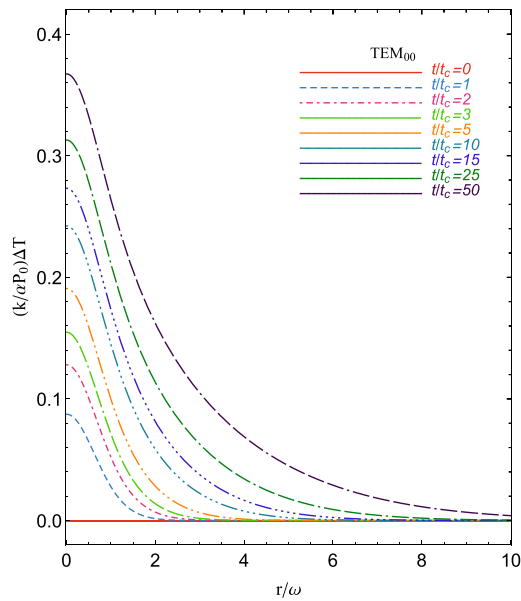


Fig. 3. Temperature profile at various times by the fundamental Gaussian mode TEM₀₀.

$$I_0^2 = \frac{8P_0}{\pi} \frac{r^4}{w^6} \exp\left(\frac{-2r^2}{w^2}\right), \quad (6c)$$

$$I_0^3 = \frac{4P_0}{\pi} \frac{r^6}{w^8} \exp\left(\frac{-2r^2}{w^2}\right), \quad (6d)$$

$$I_0^4 = \frac{2P_0}{\pi} \frac{r^8}{w^{10}} \exp\left(\frac{-2r^2}{w^2}\right), \quad (6e)$$

$$I_0^5 = \frac{64P_0}{\pi} \frac{r^{10}}{w^{12}} \exp\left(\frac{-2r^2}{w^2}\right). \quad (6f)$$

The relative intensities of Gaussian and various LG modes that we use as excitation sources are plotted in Fig. 2. All the

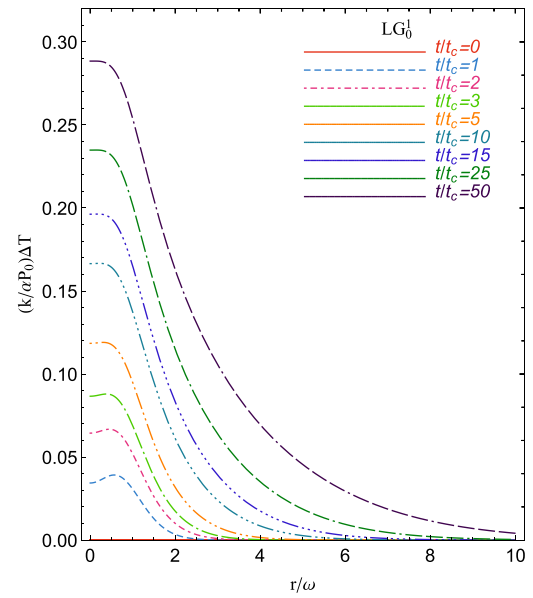


Fig. 4. Temperature profile at various times by LG₀¹.

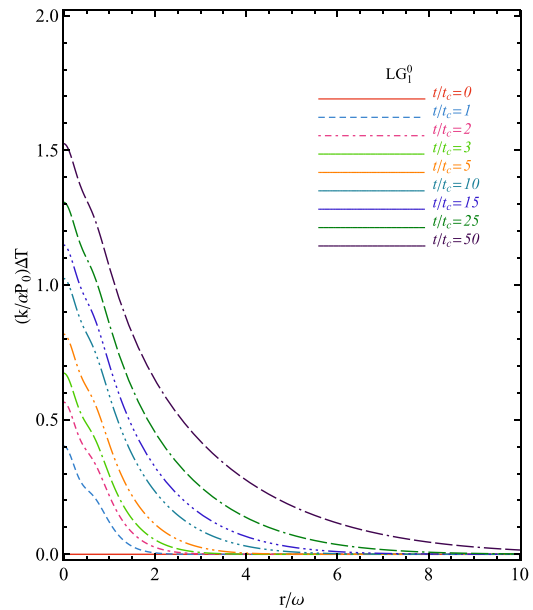


Fig. 5. Temperature profile at various times for LG₁⁰.

beam radii are normalized over the radius of TEM₀₀. Note that the intensity profile of the LG₁⁰ mode presents the narrowest radius that can generate a higher refractive index gradient than any other intensity profile.

Gordon *et al.* [7] calculated the associated temperature profile generated by the intensity profile of TEM₀₀:

$$\Delta T = \frac{\alpha P_0}{4k\pi} \left[\text{Ei}\left(-2r^2/w^2\right) - \text{Ei}\left(-\frac{2r^2/w^2}{2t/t_c + 1}\right) \right]. \quad (7)$$

The radial temperature profile generated by the Gaussian mode is depicted in Fig. 3. It can be seen that temperature drops rapidly outside the beam, irrespective of time [7].

For the excitation mode of LG_0^1 , the temperature rise is calculated using Eq. (6a) by substituting the value of intensity in the source term given in Eq. (5), and we get

$$\Delta T = \int_0^t \int_0^\infty \left(\frac{4P_0}{\pi} \frac{2\pi\alpha}{4\pi t'k} \right) \exp\left(-\frac{r_1^2 + r^2}{4Dt'}\right) I_0\left(\frac{2rr_1}{2Dt'}\right) \frac{r_1^3}{w^2} \exp\left(\frac{-2r_1^2}{w^2}\right) dr_1 dt'. \quad (8)$$

To solve Eq. (5) for r_1 , we use the following integration result:

$$\int_0^\infty r^3 \cdot \exp(-p^2 r^2) \cdot I_0(br) dr = \exp\left(\frac{b^2}{4p^2}\right) \cdot \frac{b^2 + 4p^2}{8p^6}. \quad (9)$$

Absorbing all constants in c and performing the integration on t' gives the following result:

$$\Delta T = c \cdot \frac{D}{k} \left[\frac{-e^{-\frac{2r^2}{w^2}} - \text{Ei}\left(-\frac{2r^2}{w^2}\right)}{16D} + \frac{w^2 e^{-\frac{2r^2}{8Dt+w^2}} - (8Dt+w^2)\text{Ei}\left(\frac{-2r^2}{8Dt+w^2}\right)}{16D(8Dt+w^2)} \right]. \quad (10)$$

Now we introduce a new parameter, $t_c = \frac{w^2}{4D}$, the buildup time for TL, called characteristic thermal time constant, and the result becomes

$$\Delta T = \frac{\alpha P_0}{4 \cdot k \cdot \pi} \left[-e^{-2r^2/w^2} + \frac{e^{-\frac{2r^2/w^2}{2t/t_c+1}}}{2t/t_c+1} + \text{Ei}(-2r^2/w^2) - \text{Ei}\left(\frac{2r^2/w^2}{2t/t_c+1}\right) \right], \quad (11)$$

where Ei is defined as an exponential integral [23].

Figure 4 illustrates the relative temperature field profile for LG_0^1 excitation mode during heating of the sample; the x axis is normalized over the radius of the beam. At lower values of t/t_c , it resembles the profile of the excitation beam. At later times, there is a broadening of the temperature profile due to thermal diffusion length, and the central part reaches a plateau with flat, constant intensity. The shape of the profile continues to grow, but it remains the same, and the temperature gradient vanishes as we move away from the central part.

Using a full width at half maxima (FWHM) technique, we calculated the numerical ratio of radius of TEM_{00} to LG_0^1 , which is equal to $\omega = \omega_0/1.8$, and ω_0 is the radius of TEM_{00} . The calculations of temperature gradient for the LG_0^1 excitation beam is given as

$$\Delta T = \frac{\alpha P_0}{8k\pi} \left[-e^{-2r^2/w^2} \left(\frac{2r^2}{w^2} + 1 \right) + e^{-\frac{2r^2/w^2}{2t/t_c+1}} \left(\frac{2r^2}{w^2} + \left(\frac{2t}{t_c} + 1 \right) \left(\frac{4t}{t_c} + 1 \right) \right) \frac{1}{(2t/t_c+1)^2} + \text{Ei}(-2r^2/w^2) - \text{Ei}\left(\frac{2r^2/w^2}{2t/t_c+1}\right) \right]. \quad (12)$$

In Fig. 5, the temperature profile produced by the LG_0^1 excitation mode is presented. If we compare Figs. 3 and 5, it can be seen that the temperature profile generated by LG_0^1 is narrower than the profile generated by the TEM_{00} mode. However, the intensity is higher in the central part near the axis, enabling a higher temperature gradient along the radius.

The temperature gradient produced in the sample for LG_0^2 is calculated with the use of Eq. (6b) in Eq. (5):

$$\Delta T = \frac{\alpha P_0}{4 \cdot k \cdot \pi} \left[-e^{-2r^2/w^2} \left(\frac{2r^2}{w^2} + 3 \right) + e^{-\frac{2r^2/w^2}{2t/t_c+1}} \left(\frac{2r^2}{w^2} + \left(\frac{2t}{t_c} + 1 \right) \left(\frac{8t}{t_c} + 3 \right) \right) \frac{r^2}{w^2} + 2\text{Ei}(-2r^2/w^2) - 2\text{Ei}\left(\frac{2r^2/w^2}{2t/t_c+1}\right) \right]. \quad (13)$$

Similarly, we can derive the temperature rise for excitation mode LG_0^3 as follows:

$$\Delta T = \frac{\alpha P_0}{4 \cdot k \cdot \pi} \left[\frac{-e^{-2r^2/w^2} \left(\frac{4r^4}{w^4} + 10 \frac{r^2}{w^2} + 11 \right) + \frac{e^{-\frac{2r^2/w^2}{2t/t_c+1}}}{(2t/t_c+1)^5} \left(4 \frac{r^4}{w^4} + 2 \frac{r^2}{w^2} \left(\frac{2t}{t_c} + 1 \right) \left(18 \frac{t}{t_c} + 5 \right) + \left(\frac{2t}{t_c} + 1 \right)^2 \left(72 \left(\frac{t}{t_c} \right)^2 + 54 \frac{t}{t_c} + 11 \right) \right)}{6\text{Ei}(-2r^2/w^2) - 6\text{Ei}\left(\frac{2r^2/w^2}{2t/t_c+1}\right)} \right]. \quad (14)$$

The analytic calculations for temperature rise due to modes LG_0^4 and LG_0^5 , respectively, are derived as

$$\Delta T = \frac{\alpha P_0}{2 \cdot k \cdot \pi} \left[\frac{-e^{-2r^2/w^2} \left(4 \frac{r^6}{w^6} + 14 \frac{r^4}{w^4} + 26 \frac{r^2}{w^2} + 25 \right) + \frac{e^{-\frac{2r^2/w^2}{2t/t_c+1}}}{(2t/t_c+1)^7} \left(4 \frac{r^6}{w^6} + 2 \frac{r^4}{w^4} \left(\frac{2t}{t_c} + 1 \right) \left(32 \frac{t}{t_c} + 7 \right) + 2 \frac{r^2}{w^2} \left(\frac{2t}{t_c} + 1 \right)^2 \left(144 \left(\frac{t}{t_c} \right)^2 + 80 \frac{t}{t_c} + 13 \right) + \left(\frac{2t}{t_c} + 1 \right)^3 \left(384 \left(\frac{t}{t_c} \right)^3 + 432 \left(\frac{t}{t_c} \right)^2 + 176 \frac{t}{t_c} + 25 \right) \right)}{+12\text{Ei}(-2r^2/w^2) - 12\text{Ei}\left(\frac{2r^2/w^2}{2t/t_c+1}\right)} \right], \quad (15)$$

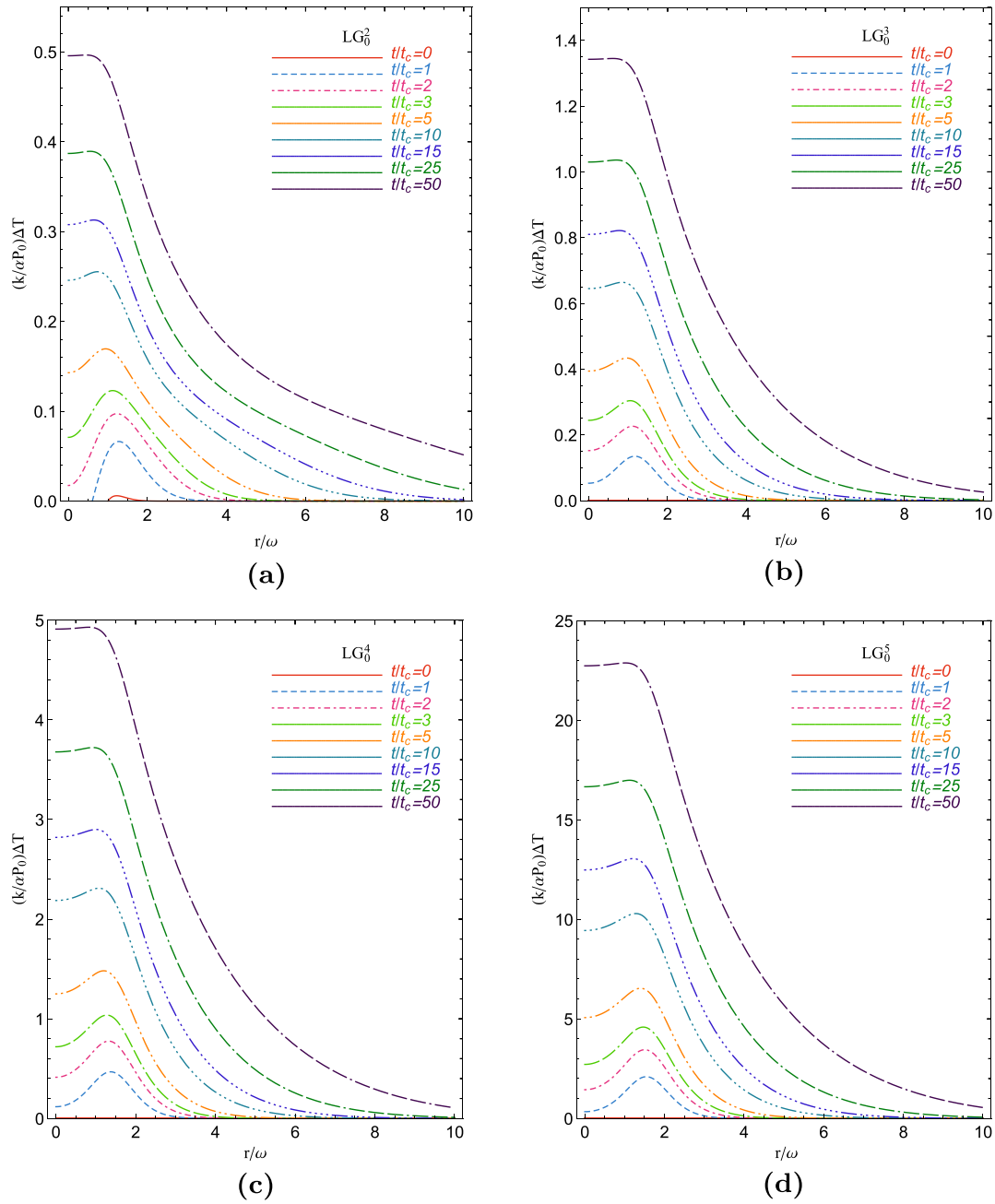


Fig. 6. Temperature profiles at various times for (a) LG_0^2 , (b) LG_0^3 , (c) LG_0^4 , and (d) LG_0^5 .

$$\Delta T = \frac{\alpha P_0}{2 \cdot k \cdot \pi} \left[+ \frac{e^{-2r^2/w^2}}{(2t/t_c+1)^9} \left(\begin{aligned} & -e^{-2r^2/w^2} \left(8 \frac{r^8}{w^8} + 36 \frac{r^6}{w^6} + 94 \frac{r^4}{w^4} + 154 \frac{r^2}{w^2} + 137 \right) \right. \\ & \left(\left(8 \frac{r^8}{w^8} + 4 \frac{r^6}{w^6} \left(2 \frac{t}{t_c} + 1 \right) \left(50 \frac{t}{t_c} + 9 \right) + 2 \frac{r^4}{w^4} \left(2 \frac{t}{t_c} + 1 \right)^2 \left(800 \left(\frac{t}{t_c} \right)^2 + 350 \frac{t}{t_c} + 47 \right) + \right. \right. \\ & \left. \left. 2 \frac{r^2}{w^2} \left(2 \frac{t}{t_c} + 1 \right)^3 \left(2400 \left(\frac{t}{t_c} \right)^3 + 2000 \left(\frac{t}{t_c} \right)^2 + 650 \frac{t}{t_c} + 77 \right) \right. \right. \\ & \left. \left. + \left(2 \frac{t}{t_c} + 1 \right)^4 \left(8400 \left(\frac{t}{t_c} \right)^4 + 7200 \left(\frac{t}{t_c} \right)^3 + 4400 \left(\frac{t}{t_c} \right)^2 + 1250 \frac{t}{t_c} + 137 \right) \right. \right. \\ & \left. \left. + 60 \text{Ei}(-2r^2/w^2) - 60 \text{Ei} \left(\frac{2r^2/w^2}{2t/t_c+1} \right) \right) \right] \quad (16) \end{aligned} \right.$$

The temperature profiles for the higher-order Gaussian modes LG_0^2 , LG_0^3 , LG_0^4 , LG_0^5 are plotted in Fig. 6.

Note that the temperature rise along the optical axis increases with the order of the high Gaussian mode. Interestingly, the central part is converted into flat intensity when t increases. The central intensity at $r/w = 0$ reaches its maximum value only in a steady state situation ($t \gg t_c$), and this value is related to the thermal diffusivity of the sample used as the absorbing medium. As we can see, generated temperature profiles of the TEM₀₀ and LG₁⁰ (Fig. 3, Fig. 5) match pretty well with their intensity profiles.

$$n(r, t) = 1.36 - \frac{\alpha P_0}{8 \cdot k \cdot \pi} \left[-e^{-2r^2/w^2} \left(\frac{2r^2}{w^2} + 1 \right) + e^{-\frac{2r^2/w^2}{2t/t_c+1}} \left(\frac{2r^2}{w^2} + \frac{(2t/t_c+1)(4t/t_c+1)}{(2t/t_c+1)^2} \right) + \text{Ei}(-2r^2/w^2) - \text{Ei} \left(\frac{2r^2/w^2}{2t/t_c+1} \right) \right]. \quad (20)$$

$$n(r, t) = 1.36 - \frac{\alpha P_0}{2 \cdot k \cdot \pi} (4 \times 10^{-4})$$

$$\times \left[\begin{aligned} & -e^{-2r^2/w^2} \left(8 \frac{r^8}{w^8} + 36 \frac{r^6}{w^6} + 94 \frac{r^4}{w^4} + 154 \frac{r^2}{w^2} + 137 \right) \\ & \left(\left(8 \frac{r^8}{w^8} + 4 \frac{r^6}{w^6} \left(2 \frac{t}{t_c} + 1 \right) \left(50 \frac{t}{t_c} + 9 \right) + 2 \frac{r^4}{w^4} \left(2 \frac{t}{t_c} + 1 \right)^2 \left(800 \left(\frac{t}{t_c} \right)^2 + 350 \frac{t}{t_c} + 47 \right) + \right. \right. \\ & \left. \left. 2 \frac{r^2}{w^2} \left(2 \frac{t}{t_c} + 1 \right)^3 \left(2400 \left(\frac{t}{t_c} \right)^3 + 2000 \left(\frac{t}{t_c} \right)^2 + 650 \frac{t}{t_c} + 77 \right) \right. \right. \\ & \left. \left. + \left(2 \frac{t}{t_c} + 1 \right)^4 \left(8400 \left(\frac{t}{t_c} \right)^4 + 7200 \left(\frac{t}{t_c} \right)^3 + 4400 \left(\frac{t}{t_c} \right)^2 + 1250 \frac{t}{t_c} + 137 \right) \right. \right. \\ & \left. \left. + 60 \text{Ei}(-2r^2/w^2) - 60 \text{Ei} \left(\frac{2r^2/w^2}{2t/t_c+1} \right) \right) \right]. \quad (21) \end{aligned}$$

4. REFRACTIVE INDEX DISTRIBUTION PRODUCED BY LG MODES

In this section, we discuss refractive index profiles associated with the temperature gradients of LG_p^l modes discussed in Section 3. The refractive index distribution [7] can be written as

$$n(r, t) = n_0 + \left(\frac{\partial n}{\partial T} \right) \Delta T(r, t) + \left(\frac{\partial^2 n}{\partial T^2} \right) \Delta T(r, t)^2 + \dots, \quad (17)$$

where n_0 is the refractive index at the initial temperature T_0 . We restrict our analysis to liquids, and only the first order in Eq. (17) is considered. For these systems, the refractive index decreases with increasing temperature [see Eq. (18)], thus producing a diverging lens effect since the refractive index is lower on the beam axis than on the edges:

$$n(r, t) = n_0 - \left(\frac{dn}{dT} \right) \Delta T(r, t). \quad (18)$$

Now we briefly discuss some orders of LG propagating in a solvent such as ethanol for which the values of the refractive index n_0 and refractive index gradient $\frac{dn}{dT}$ (at 300 K) are 1.36 and $4 \times 10^{-4} \text{ K}^{-1}$, respectively [24]. The refractive index distribution for the Gaussian mode can be solved by using Eq. (6) and Eq. (18) and is written as

$$n(r, t) = 1.36 - \frac{\alpha P_0}{4 \cdot k \cdot \pi} \left(4 \times 10^{-4} \right) \times \left[\text{Ei}(-2r^2/w^2) - \text{Ei} \left(-\frac{2r^2/w^2}{2t/t_c+1} \right) \right]. \quad (19)$$

The refractive index distribution produced by the Gaussian mode is plotted using Eq. (19), as shown in Fig. 7. For mode LG₁⁰, the refractive index distribution according to intensity given in Eq. (6b) and using Eq. (18) is given by

Likewise, the gradient of the refractive index for LG₀⁵ can be written by employing Eq. (16) in Eq. (18):

Figures 8 and 9 show the refractive index distribution by higher modes LG₁⁰ and LG₀⁵, respectively. The refractive index gradient in a steady state situation $t \gg t_c$, along the radius of the fundamental Gaussian mode, is lower than the refractive index gradient produced by the higher-order Gaussian mode LG₀⁵.

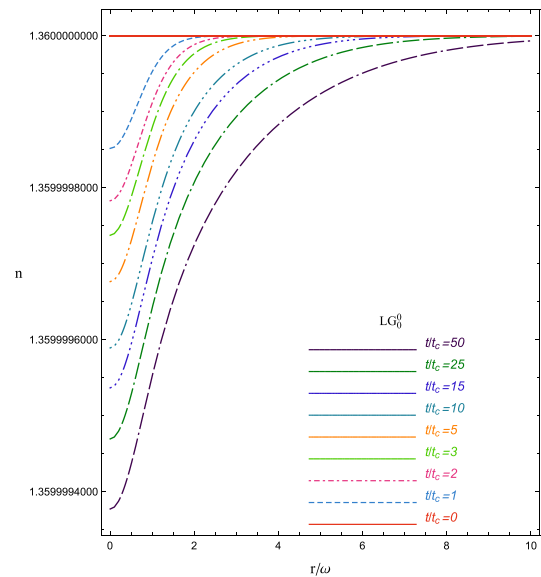


Fig. 7. Refractive index profile by Gaussian mode excitation beam profile for ethanol with absorption coefficient $\alpha = 5.9 \times 10^{-4} \text{ cm}^{-1}$, power 12 mW, and thermal conductivity $1.67 \times 10^{-3} \text{ W} \cdot \text{cm}^{-1} \cdot \text{K}^{-1}$ [3].

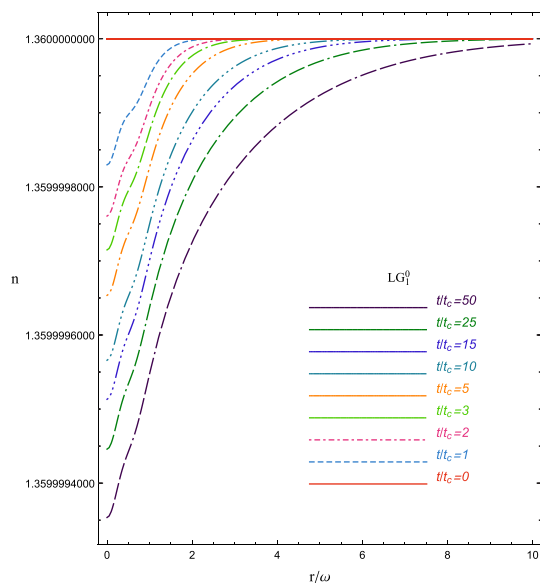


Fig. 8. Refractive index profile for LG_1^0 , for ethanol with absorption coefficient $\alpha = 5.9 \times 10^{-4} \text{ cm}^{-1}$, power 12 mW, and thermal conductivity $1.67 \times 10^{-3} \text{ W} \cdot \text{cm}^{-1} \cdot \text{K}^{-1}$.

An increase in the refractive index gradient enables to produce a high TL signal and sensitivity under the same experimental conditions but working only at very low chopping frequencies to reach the steady state condition ($t \gg t_c$). Another additional interesting characteristic of the refractive index profile produced by the higher-order Gaussian beam LG_0^5 is that the flat region around the optical axis is extended. This fact enables that the area of maximal TL signal is also extended; thus, the dimensions of the pinhole are not so critical as in the case of Gaussian beam excitation. Collectively, these results suggest a higher sensitivity for measurement. Moreover, the refractive index gradient of

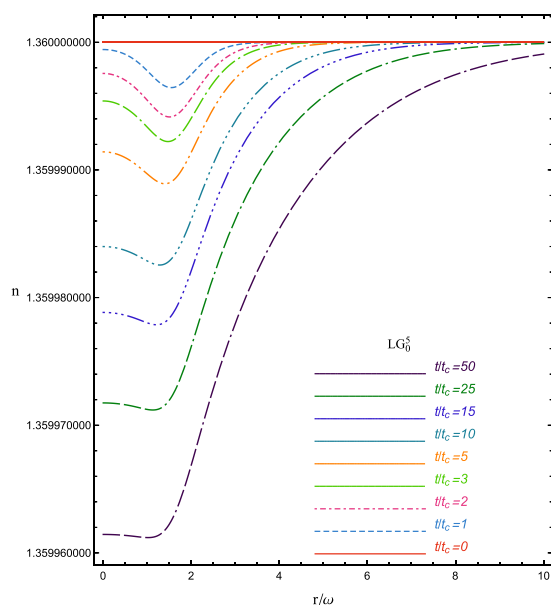


Fig. 9. Refractive index profile for LG_0^5 , for ethanol with absorption coefficient $\alpha = 5.9 \times 10^{-4} \text{ cm}^{-1}$, power 12 mW, and thermal conductivity $1.67 \times 10^{-3} \text{ W} \cdot \text{cm}^{-1} \cdot \text{K}^{-1}$.

LG_1^0 along the radius is higher than the refractive index gradient of TEM_{00} even at lower illumination times. Collectively, these results suggest higher sensitivity using lower excitation power.

5. CONCLUSION

In this paper, we have investigated the temperature and refractive index profiles when the TL effect is generated by LG modes of excitation laser beams such as LG_1^0 , LG_0^1 , LG_0^2 , LG_0^3 , LG_0^4 , and LG_0^5 . The analysis has been performed based on the radial dependence of the temperature and refractive index profiles generated by LG beams after different times. The temperature and refractive index profiles spread following the thermal diffusion length, which depends on the thermal diffusivity of the medium. Moreover, the shape of each profile resembles the shape of the specific LG mode used as the excitation beam. An increase in the angular modes of the excitation laser ($l = 1, 2, 3 \dots$) produces an upward shift of the temperature profile under a steady state condition. A comparison with the fundamental Gaussian beam TEM_{00} indicates that the temperature gradient in the vicinity of the axis can be increased substantially when using higher-order Gaussian modes but only if the steady state condition is reached. However, for LG_1^0 , the refractive index gradient is higher than for TEM_{00} even at lower illumination times. This fact can contribute to generate a high TL signal as well as high sensitivity in measurement. In perspective, this result can be used for further development of a TL model based on non-Gaussian excitation beams such as LG, which can be easily generated using different optical elements. This work is in progress along with the correspondent experimental procedure.

Acknowledgment. Dr. Imrana Ashraf expresses gratitude to the Associate office at The Abdus Salam International Centre for Theoretical Physics (ICTP) for supporting her last associate visit. Additionally, Dr. Humberto Cabrera acknowledges the support received from the SPIE-ICTP Anchor Research Program funded generously by the International Society for Optics and Photonics (SPIE) as well as the ICTP for support of work through the OEA Office.

Disclosures. The authors declare no conflicts of interest.

REFERENCES

1. M. Proskurnin, D. Volkov, T. Gorkova, S. Bendrysheva, A. Smirnova, and D. Nedosekin, "Advances in thermal lens spectrometry," *J. Anal. Chem.* **70**, 249–276 (2015).
2. C. D. Tran and M. Franko, "Thermal lens spectroscopy," in *Encyclopedia of Analytical Chemistry*, R. A. Meyers, ed. (Wiley, 2010).
3. H. Cabrera, J. Akbar, D. Korte, I. Ashraf, E. E. Ramirez-Miquet, E. Marin, and J. Niemela, "Absorption spectra of ethanol and water using a photothermal lens spectrophotometer," *Appl. Spectrosc.* **72**, 1069–1073 (2018).
4. R. L. Swofford, M. E. Long, and A. C. Albrecht, "C–H vibrational states of benzene, naphthalene, and anthracene in the visible region by thermal lensing spectroscopy and the local mode model," *J. Chem. Phys.* **65**, 179–190 (1976).
5. S. M. Lima, J. A. Sampaio, T. Catunda, A. C. Bento, L. C. M. Miranda, and M. L. Baesso, "Mode-mismatched thermal lens spectrometry for

- thermo-optical properties measurement in optical glasses: a review," *J. Non Cryst. Solids* **273**, 215–227 (2000).
6. H. Cabrera, D. Mendoza, J. L. Benitez, C. B. Flores, S. Alvarado, and E. Marín, "Thermal diffusivity of few-layers graphene measured by an all-optical method," *J. Phys. D* **48**, 465501 (2015).
 7. J. P. Gordon, R. C. C. Leite, R. S. Moore, S. P. S. Porto, and J. R. Whinnery, "Long-transient effects in lasers with inserted liquid samples," *J. Appl. Phys.* **36**, 3–8 (1965).
 8. C. Hu and J. R. Whinnery, "New thermo-optical measurement method and a comparison with other methods," *Appl. Opt.* **12**, 72–79 (1973).
 9. D. Solimini, "Loss measurement of organic materials at 6328 Å," *J. Appl. Phys.* **37**, 3314–3315 (1966).
 10. F. R. Grabiner, D. R. Siebart, and G. W. Flynn, "Laser induced time-dependent thermal lensing studies of vibrational relaxation: translational cooling in CH₃F," *Chem. Phys. Lett.* **17**, 189–194 (1972).
 11. H. Cabrera, J. Akbar, D. Korte, E. E. Ramírez-Miquet, E. Marín, J. Niemela, Z. Ebrahimpour, K. Mannatunga, and M. Franko, "Trace detection and photothermal spectral characterization by a tuneable thermal lens spectrometer with white-light excitation," *Talanta* **183**, 158–163 (2018).
 12. M. Franko and C. D. Tran, "Thermal lens spectroscopy electronic absorption and luminescence," in *Encyclopedia of Analytical Chemistry: Applications, Theory and Instrumentation* (2010).
 13. Y. Ohtake, T. Ando, N. Fukuchi, N. Matsumoto, H. Ito, and T. Hara, "Universal generation of higher order multiringed Laguerre-Gaussian beams by using a spatial light modulator," *Opt. Lett.* **32**, 1411–1413 (2007).
 14. T. Ando, Y. Ohtake, N. Matsumoto, T. Inoue, and N. Fukuchi, "Mode purities of Laguerre Gaussian beams generated via complex-amplitude modulation using phase-only spatial light modulators," *Opt. Lett.* **34**, 34–36 (2009).
 15. L. Carbone, P. Fulda, C. Bond, F. Brueckner, D. Brown, M. Wang, D. Lodhia, R. Palmer, and A. Freise, "The generation of higher-order Laguerre–Gauss beams for high-precision interferometry," *J. Visual. Exp.* **78**, 50564 (2013).
 16. R. Steiger, S. Bernet, and M. Ritsch-Marte, "Mapping of phase singularities with spiral phase contrast microscopy," *Opt. Express* **21**, 16282–16289 (2013).
 17. C. H. Chen, P. T. Tai, and W. F. Hsieh, "Bottle beam from a bare laser for single-beam tapping," *Appl. Opt.* **43**, 6001–6006 (2004).
 18. S. W. Hell and J. Wichmann, "Breaking the diffraction resolution limit by stimulated emission: stimulated-emission-depletion fluorescence microscopy," *Opt. Lett.* **19**, 780–782 (1994).
 19. A. Bencheikh, M. Fromager, and K. Aït-Ameur, "Extended focus depth for Gaussian beam using binary phase diffractive optical elements," *Appl. Opt.* **57**, 1899–1903 (2018).
 20. L. C. Davila-Romero, D. L. Andrews, and M. Babiker, "A quantum electrodynamics framework for the nonlinear optics of twisted beams," *J. Opt. B Quantum Semiclass. Opt.* **4**, S66 (2002).
 21. R. Dennemeyer and P. L. Balise, "Introduction to partial differential equations and boundary value problems," *Phys. Today* **21**(12), 85 (1968).
 22. H. S. Carslaw and J. C. Jaeger, *Operational Methods in Applied Mathematics*, 2nd ed. (Dover Publications, 1948).
 23. E. Jahnke and F. Emde, *Tables of Functions* (Teubner, 1938), pp. 1–8.
 24. H. Cabrera, A. Marcano, and Y. Castellanos, "Absorption coefficient of nearly transparent liquids measured using thermal lens spectrometry," *Condens. Matter Phys.* **9**, 385–389 (2006).